Supporting Information

For

Boron-enrichment Rice-homologous Carbon Nanoclusters with a 51.5% Photoluminescent Quantum Yield for Highly Sensitive Determination of Endogenous Hydroxyl Radical in Living Cells

Zhong-Xia Wang,[a] Lei Hu,[a] Xiao-Qiong Li,[b] Yi-Lei Jia,[b] Ting Wang,[b] and Wei Wang*[a]*

[a] *School of Chemistry and Chemical Engineering, Yancheng Institute of Technology, Yancheng 224051, China.*

[b] *State Key Laboratory of Analytical Chemistry for Life Science, School of Chemistry and Chemical Engineering, Nanjing University, Nanjing 210023, China.*

***Corresponding authors**. (Z.X. Wang) Tel. (Fax): +86-515-88298186.*

E-mail: Wei Wang: wangw@ycit.edu.cn;

Zhong-Xia Wang: wangzx198411@163.com.

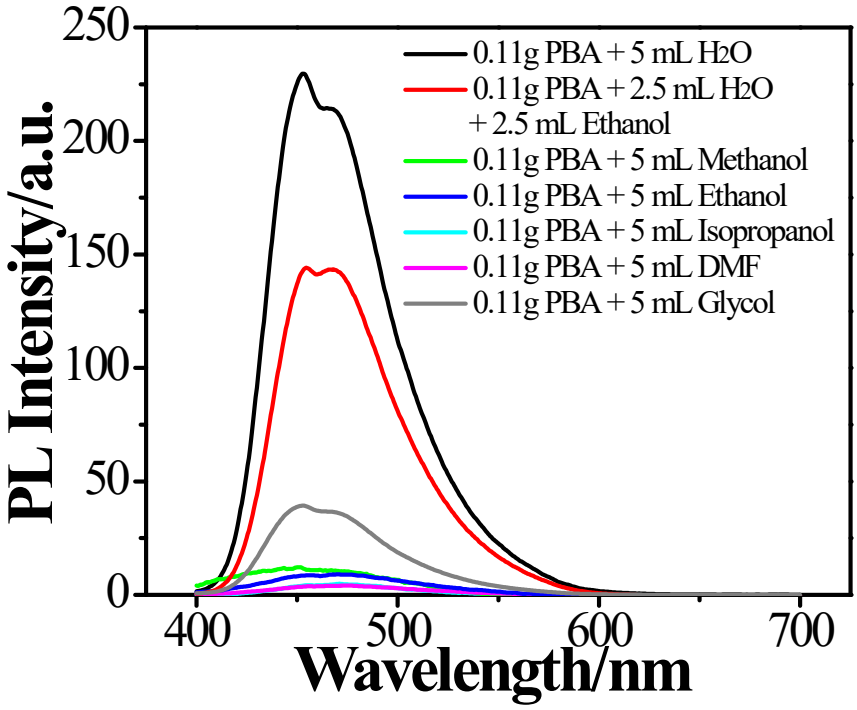

Figure S1 Effect of the solvents (the mass of PBA precursor was all 110 mg) on the PL intensity of the carbon nanomaterial (λex=390 nm), and the excitation and emission slit widths were 10 nm and 1 nm, respectively.

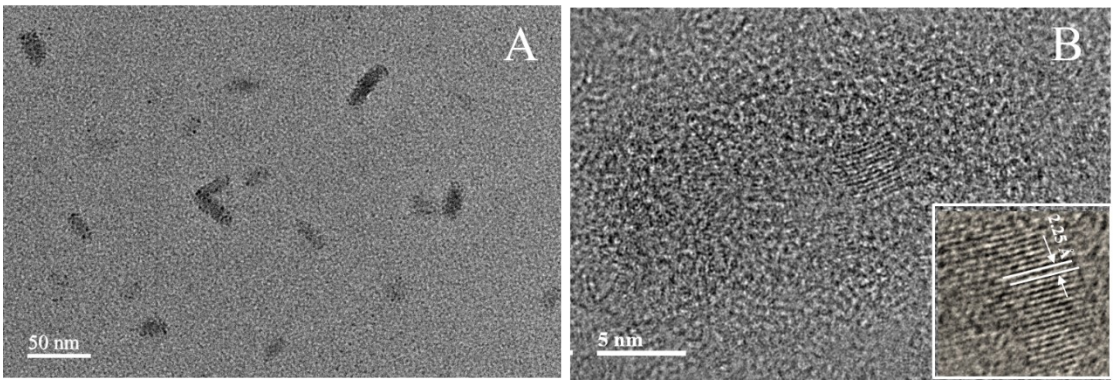

Figure S2 TEM (A) and HRTEM (B) images of the BRCNs.

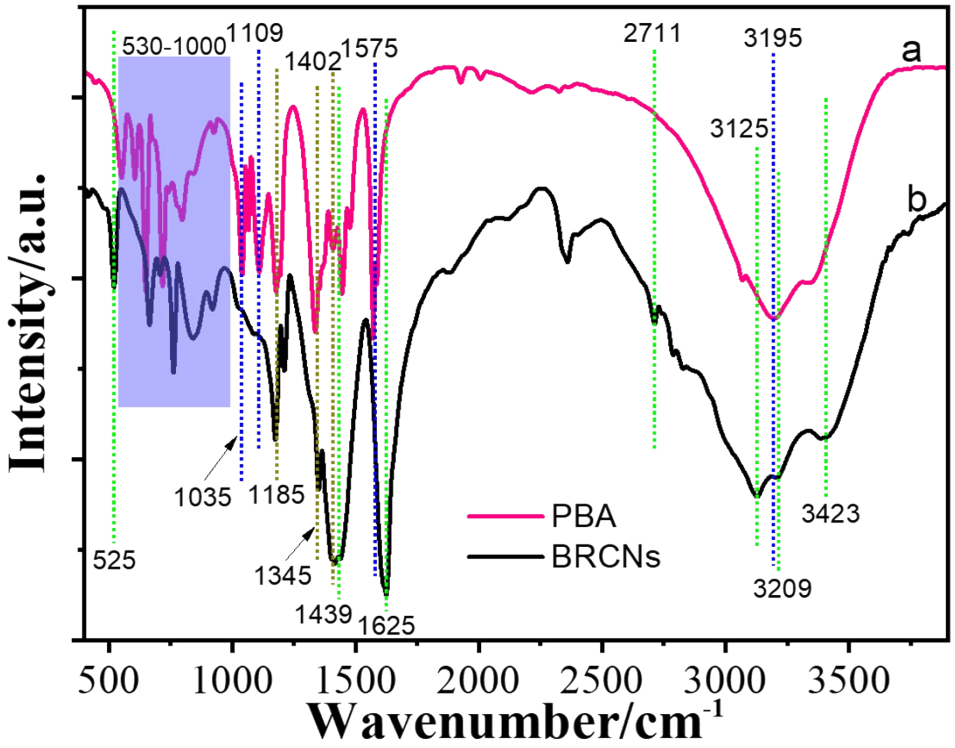

Figure S3 FT-IR spectra of the PBA (line a) and BRCNs (line b). Green dot-line represents new peaks, the blue dot-line represents disappeared or moved peaks, and the gray dot-line represents coexisting peaks.

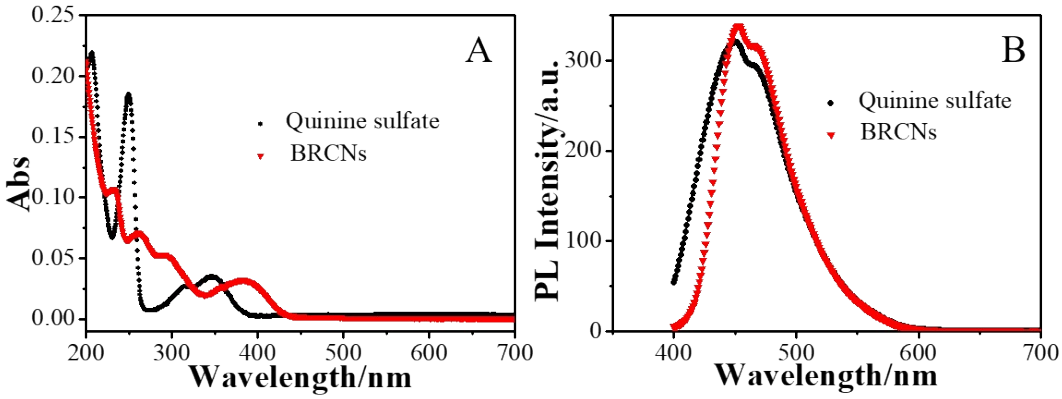

Figure S4 UV-vis absorption (A) and PL emission spectra (B) exited at 360 nm of BRCNs in water (▼) and quinine sulfate (●) in 0.1 M H_2SO_4 solution as the standard. The asymmetry of BRCNs emission spectra may be caused by the re-absorption in the blue part of the spectra.

Quantum Yield Measurements.

Reference on quantum yield measurements: Lakowicz, J. R. *Rinciples of Fluorescence Spectroscopy*, 2nd Ed., **1999**, Kluwer Academic/Plenum Publishers, New York. The optical densities were measured on a Shimadzu UV-2550 spectrophotometer (Tokyo, Japan) in the range of 200-700 nm. Quinine sulfate in 0.1 M H_2SO_4 (literature quantum yield 0.54 at 360 nm) was chosen as a standard. Absolute values are calculated using the standard reference sample that has a fixed and known fluorescent quantum yield value, according to the following equation:

$$\Phi_x = \Phi_s \left[\frac{Fu}{Au}\right] \left[\frac{As}{Fs}\right] \left[\frac{\eta u}{\eta s}\right]^2$$

where Φ is the quantum yield, *Fu* and *Fs* are the measured integrated emission intensity of BRCNs and quinine sulfate, respectively. *Au* and *As* are the optical density of BRCNs and quinine sulfate, respectively. and ηu and ηs are the refractive index of BRCNs and quinine sulfate, respectively. In order to minimize re-absorption effects absorbencies in the 10 mm fluorescent cuvette were kept under 0.05 at the excitation wavelength (360 nm).

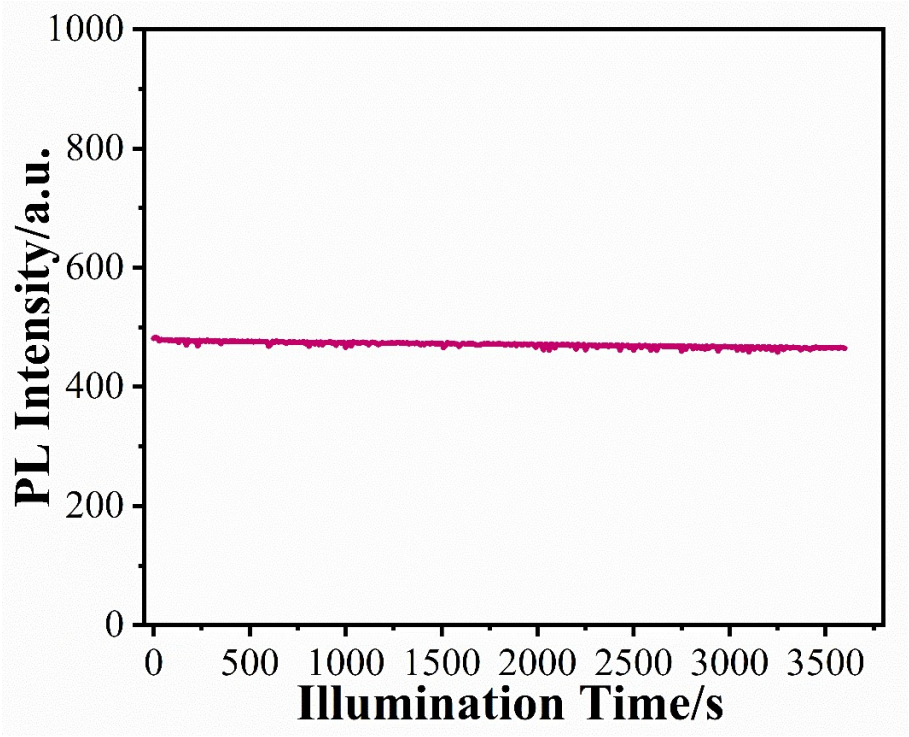

Figure S5 Photostability of BRCNs solution upon excitation for 60 min at room temperature.

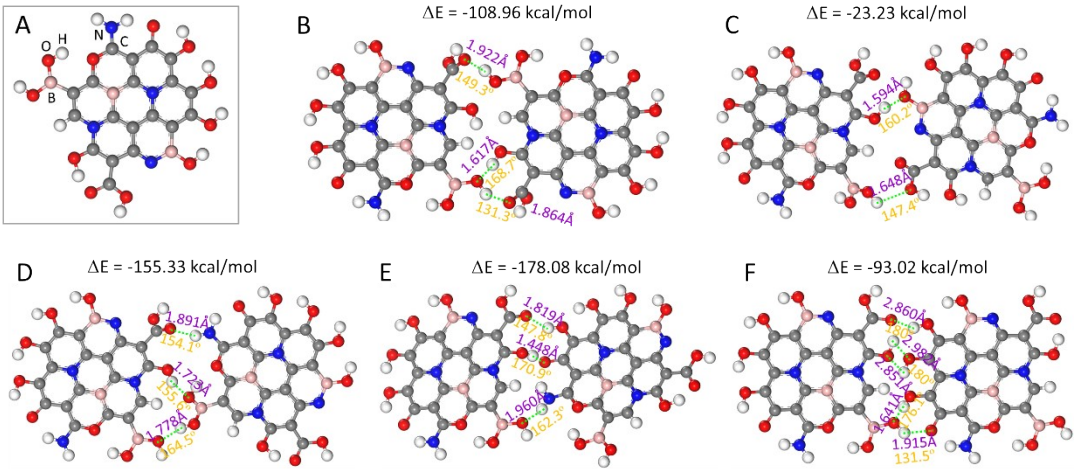

Figure S6 A) Representative functional section of denatured BRCNs (The BRCNs is reacted with OH• radicals) for calculation of H-bond properties; B-F) RB3LYP-optimized H-bonding force geometries between denatured BRCNs. Intermolecular hydrogen bonding forces are displayed as green dotted lines.

To prove the formation of H-bonds between denatured BRCNs, density functional theory (DFT) was performed. By calculating representative functional section groups on the surface of denatured BRCNs (Figure S6A, the roughly representative functional groups are generally obtained according to the characterization of material surface properties), the representative angles and lengths of H-bonds testified to the presence of the nine strong H-bonding forces between the denatured BRCNs (Figure S6B-S6F). Meanwhile, all the energy values were obtained using the optimized geometries of the nanomaterial. From Figure S6B-6F, the data showed that the ΔE of the hydrogen bonding-based nanohybrid between the denatured BRCNs were all lower than zero, suggesting denatured BRCNs prefers to produce aggregation through strong intermolecular H-bonding forces.

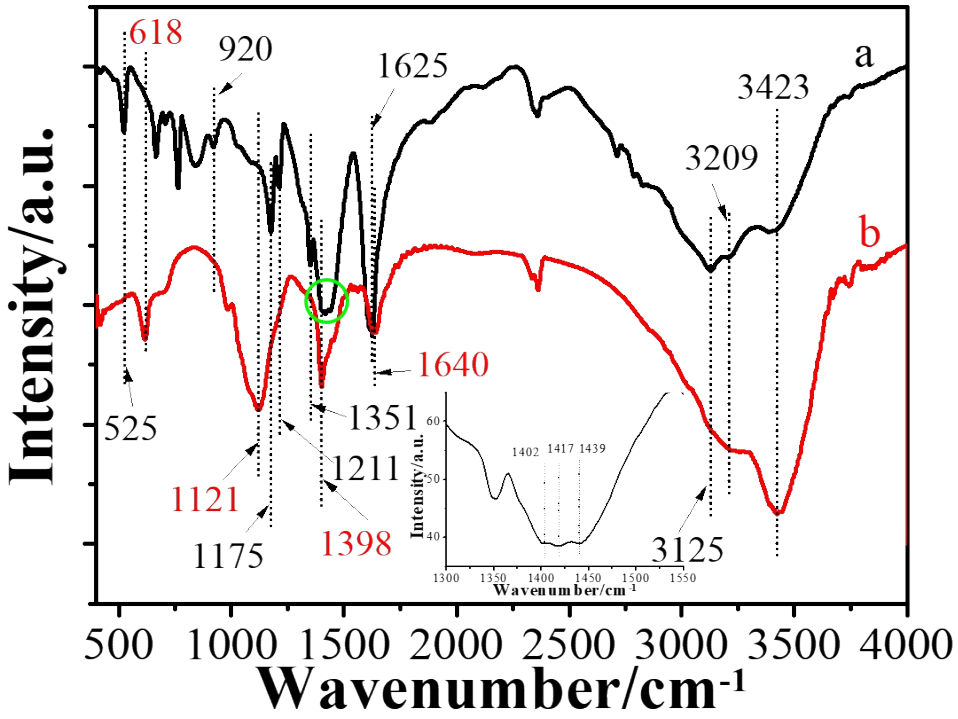

Figure S7 FT-IR spectra of the BRCNs in the absence (line a) and simultaneous presence of Fe^{2+} ion (200 μM) and H_2O_2 (50 μM) (line b); The inset below is an enlarged version of a bright green circle.

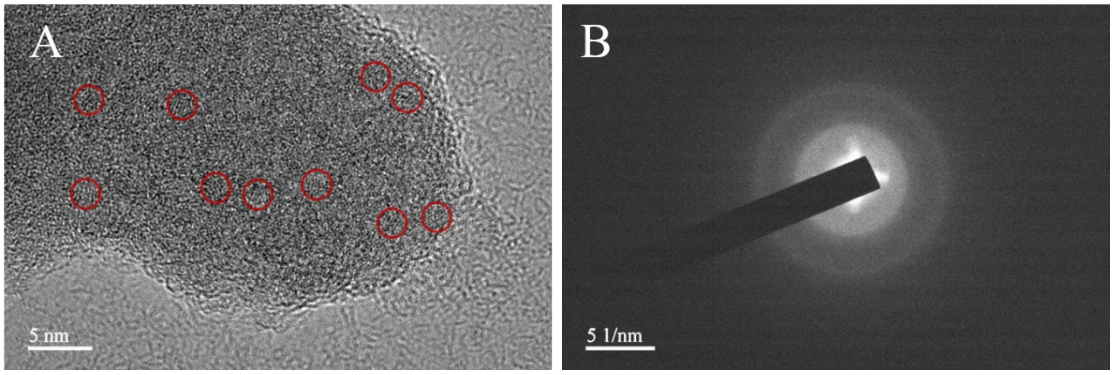

Figure S8 HRTEM (A) and SAED (B) images of the BRCNs in the presence of Fe^{2+} ion (200 μM) and H_2O_2 (100 μM). The red circle in Figure S5A is the position of the denatured BRCNs.

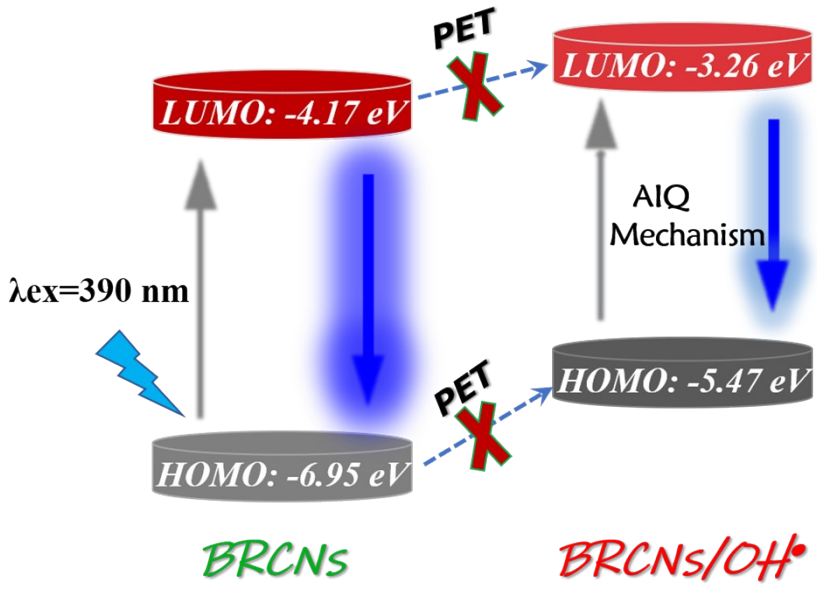

Figure S9 Schematic of PET process from BRCNs to OH• radicals.

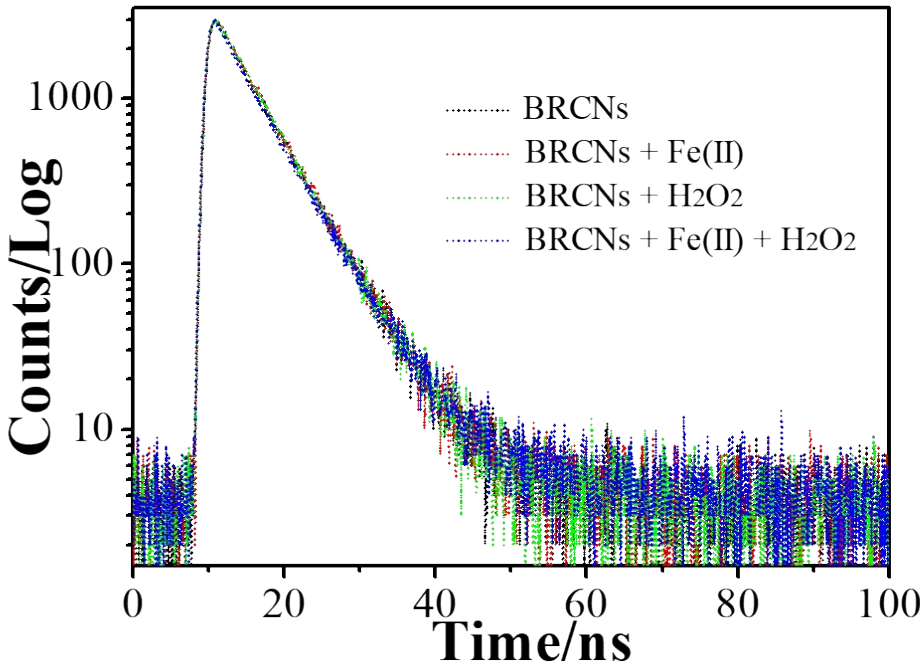

Figure S10 Decay of the PL of the BRCNs in the absence and presence of Fe^{2+} ion (200 μM), H_2O_2 (30 μM) and simultaneous presence of Fe^{2+} ion (200 μM) and H_2O_2 (30 μM).

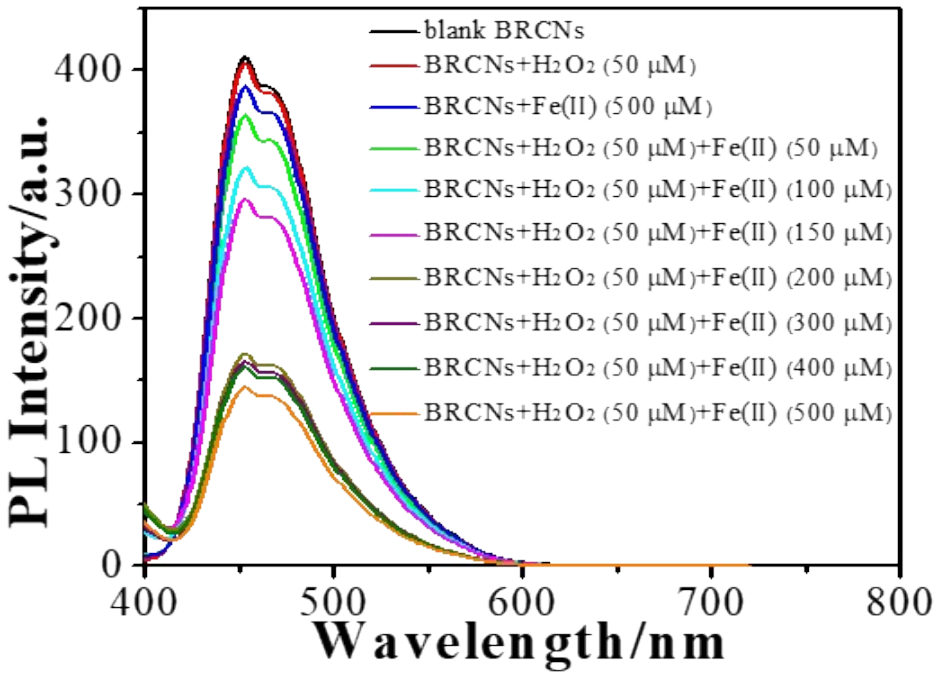

Figure S11 The PL spectra of the BRCNs in the presence of 50 μM H_2O_2 and various concentrations of Fe^{2+} ions (0 to 500.0 μM, top to bottom, excitation at 390 nm).

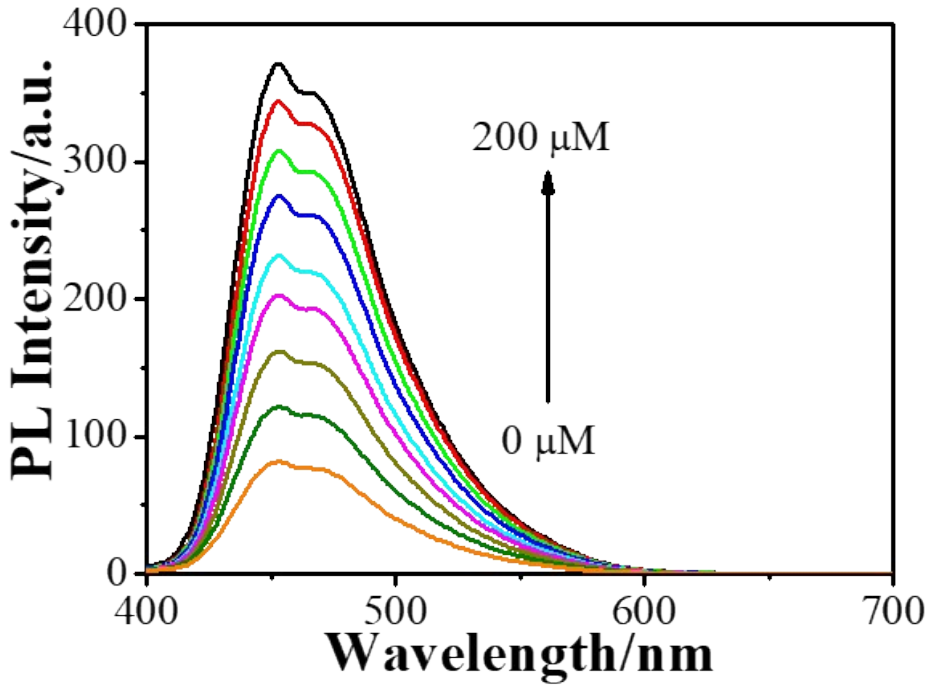

Figure S12 A) PL spectra of BRCNs after exposure to Fenton's reagent (200 μM Fe^{2+} ion, 80 μM H_2O_2) in the presence of various amounts of Vitamin C (ascorbic acid), the Vitamin C concentrations were (from bottom to top): 0, 5.0, 25, 50, 75, 100, 150 and 200 μM.

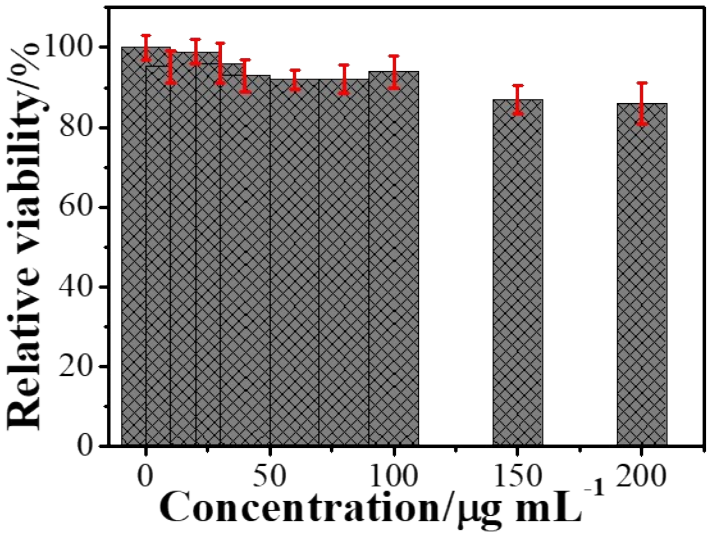

Figure S13 Viability of HeLa cells incubated with different concentrations of BRCNs (0, 10, 20, 30, 40, 60, 80, 100, 150 and 200 μg mL^{-1}) for 6 h. Data are mean ± SD (bars) (n = 3).

The study of cytotoxicity for checking the cytocompatibility of BRCNs was conducted using MTT (3-(4,5-dimethyl-2-thiazolyl)-2,5-diphenyl-2H-tetrazolium bromide) assay. In brief, HeLa cells were dispersed on 96-well plates and cultured in 100 μL of Dulbecco's Modified Eagle Medium (DMEM) containing 10% fetal bovine serum in a 5% CO_2 environment for 24 h. Next, the cells were stained with BRCNs of different concentrations (0, 10, 20, 30, 40, 60, 80, 100, 150 and 200 μg mL^{-1}) for another 6 h. Then, MTT solution (50 μL, 1 mg mL^{-1}) was added to each well, and the cells were incubated for another 4 h (37 °C, 5% CO_2). And the cells were dissolved in DMSO (150 μL $well^{-1}$), and the absorbance at 490 nm was recorded by a Thermo Scientific Varioskan Flash (Thermo Fisher Scientific, USA). All results were repeated for three times. The cell viability was estimated as the percentage of the absorbance of BRCNs treated cells to the absorbance of nontreated cells. The cell viability was estimated according to the follow equation (1):

$$\text{Cell viability (\%)} = OD_{treated}/OD_{control} \times 100\% \quad (1)$$

Where $OD_{control}$ was obtained in the absence of BRCNs and $OD_{treated}$ was obtained in the presence of BRCNs. Each measurement was performed in triplicate.

Table S1. Comparison of analyte, technology, carbon-based probes, medium, linear range and detect limit for ROS analysis using different detection method based on carbon probe.

Analyte	Technology	Carbon-based probe	Medium	Linear range	Detect limit	Ref.
ROS	Fluorescence	C-Dots-Hydrogel	HeLa cells	-	5-FU	1
OH·	Fluorescence	TPA@GQDs	HeLa cells	0.018-6 μM	12 nM	2
OH·	Fluorescence	C-Ag NPs	HeLa cells	0.25-32 μM	-	3
ROS	Fluorescence	DHLA@N-CQDs	HeLa cells	0.2-600 μM	0.12 μM	4
OH·	Fluorescence	CCA@TPP@CDs	RAW264.7 cells	0.1-160 μM	70 nM	5
OH·	Fluorescence	r-CDs	-	10-40 μM	-	6
OH·	Fluorescence	BRCNs	HeLa cells	0.1-75.0 μM	57.86 nM	This method

Table S2 The element content of the BRCNs and the BRCNs/Fe^{2+} in the presence of H_2O_2. The concentrations of Fe^{2+} and H_2O_2 were 200 μM and 50 μM, respectively.

Atomic species	***BRCNs***	***BRCNs + OH•***
	At%	At%
B	24.68	13.29
C	46.88	44.24
N	6.90	8.27
O	21.54	34.20

Table S3. Comparison of preparation method, probes, mechanism, linear range and detect limit for OH• analysis using different detection probes.

Analyte	Preparation method	Probes	Mechanism	Linear range	Detect limit	Ref.
OH•	Organic synthesis	hybrid carbazole-cyanine	Hydrogen abstraction	0-100 equiv	-	7
OH•	Organic synthesis	Rhodamine Nitroxide	Recombination of nitroxide radicals	-	1 μM	8
OH•	Organic synthesis	Organic molecule	Aromatic hydroxylation	0-60 μM	38 nM	9
OH•	Organic synthesis	Molecular probe	Oxidative dearylation	-	0.04 μM	10
OH•	Organic synthesis	MPT-Cy2	Oxidation of electron-rich heteroatoms	1-10 μM	1.16 μM	11
OH•	Organic synthesis	Cyanostilbene	Carbon bond breakage	0.1-200 μM	0.1 μM	12
OH•	Ionic crosslinking	Polymeric NPs	FRET	-	-	13
OH•	Surface modification	Quantum dots	PET	1-200 μM	0.97 μM	14
OH•	Template method	Metal nanoclusters	Template cleavage	0.05-5 μM	-	15
OH•	Ligand exchange	Upconversion NPs	FRET	4 nM-16 μM	2 nM	16
OH•	Hydrothermal synthesis	BRCNs	Aromatic hydroxylation	0.1-75.0 μM	57.86 nM	This method

Table S4 Results of the determination of $OH^{\bullet}$ radicals in serum samples (n = 3).

Sample	*Analyte*	*Initial (μM)*	*Added[a] (μM)*	*Found[a] (μM)*	*Recovery (%)*	*RSD (%)*
1#	$OH^{\bullet}$	0	10	9.47	94.70	3.87
2#	$OH^{\bullet}$	0	20	19.21	96.05	2.16
3#	$OH^{\bullet}$	0	30	30.62	102.07	2.98

[a] The data were obtained from three parallel samples.

Real samples

The bovine serum sample (BSS) was selected as the representative of real sample determination, and was obtained from Shanghai Sangon Biological Co. Ltd. (Shanghai, China). Each BSS was diluted 50-fold with HAc-NaAc buffer (pH 5.4, 10 mM), which was used for subsequent analysis. In brief, 5 μL of 1.65 mg mL^{-1} BRCNs solution, 100 μL of the diluted BSS, 100 μL Fe(II) solution (1.0 mM) and various volume of H_2O_2 standard solution (10, 20, and 30 μM) were sequentially added into a 2.0 mL centrifugal tube, which can be to generate approximately the expected quantity of $OH^{\bullet}$. After that, the above mixture was diluted to 500 μL with ultrapure water. And the diluted mixture was incubated for 20 min at room temperature, then, the PL emission spectra were recorded at λex=390 nm. The corresponding calculation rules correspond to the previous description.

Reference

1. S. Bhattacharya, R. Sarkar, S. Nandi, A. Porgador and R. Jelinek, *Anal. Chem.,* 2017, **89**, 830-836.
2. X. Hai, Z. Guo, X. Lin, X. Chen and J. Wang, *ACS Appl. Mater. Interfaces,* 2018, **10**, 5853-5861.
3. R. Wang, H. Liu, X. Meng, Y. Qian, X. Wang, F. Zhu, R. Nie and H. Wang, *J. Colloid Interf. Sci.,* 2022, **608**, 2672-2680.
4. R. Zhang and Z. Fan, *J. Lumin.,* 2021, **234**, 117998.
5. D. Zhou, H. Huang, Y. Wang, Y. Wang, Z. Hua and X. Li, *J. Mater. Chem., B* 2019, **7**, 3737-3744.
6. J. Yue, K. Zhang, H. Yu, L. Yu, T. Hou, X. Chen, H. Ge, T. Hayat, A. Alsaedi and S. Wang, *J. Mater. Sci.,* 2019, **54**, 6140-6150.
7. J.Y. Wang, Z.R. Liu, M. Ren, X. Kong, K. Liu, B. Deng and W. Lin, *Sensor. Actuat. B-Chem.*, 2016, **236**, 60-66.
8. N.B. Yapici, S. Jockusch, A. Moscatelli, S.R. Mandalapu, Y. Itagaki, D.K. Bates, S. Wiseman, K.M. Gibson, N.J. Turro and L. Bi, *Org. Lett.*, 2012, **14**, 50-53.
9. H. Li, X. Li, W. Shi, Y. Xu and H. Ma, *Angew. Chem. Int. Ed.*, 2018, **57**, 12830-12834.
10. L. Zeng, T. Xia, W. Hu, S. Chen, S. Chi, Y. Lei and Z. Liu, *Anal. Chem.*, 2018, **90**, 1317-1324.
11. F. Liu, J. Du, D. Song, M. Xu and G. Sun, *Chem. Commun.*, 2016, **52**, 4636-4639.
12. N.Y. Lim, J. Ahn, M. Won, W. Choi, J.S. Kim and J.H. Jung, *ACS Appl. Bio Mater.*, 2019, **2**, 936-942.
13. Y. Tong, X. Huang, M. Lu, B.Y. Yu, and J, Tian, *Anal. Chem.*, 2018, **90**, 3556-3562.
14. Q. Zhao, R. Zhang, D. Ye, S. Zhang, H. Chen and J. Kong, *ACS Appl. Mater. Interfaces*, 2017, **9**, 2052-2058.
15. L. Zhang, R.P. Liang, S.J. Xiao, J.M. Bai, L.L. Zheng, L. Zhan, X.J. Zhao, J.D. Qiu and C.Z. Huang, *Talanta*, 2014, *118*, 339-347.
16. Y. Liu, Q. Jia, Q. Guo, A. Jiang and J. Zhou, *Anal. Chem.*, 2017, **89**, 12299-2305.